Magneto-Structural Correlations in Linear and Bent Oxo-Bridged Transition-Metal Dimers: Comparisons, Interpretations, and Predictions of Ground-State Magnetic Properties

Högni Weihe*,‡ and Hans U. Güdel*

Contribution from the Departement für Chemie und Biochemie, Universität Bern, Freiestrasse 3, CH-3000 Bern 9, Switzerland

Received August 27, 1997

Abstract: The angular dependence of the magnetic properties of all known octahedrally coordinated oxo-bridged dimers with trivalent 3d transition metals are interpreted in terms of the most simple concepts. These concepts are based on a combination of kinetic exchange and the chemically intuitive angular overlap model. The use of an angular overlap model allows the separation of the σ donor properties of the bridging oxide ligand into sσ and pσ contributions. An estimate of the sσ and the pσ angular overlap model parameters is given. An analysis of the magnetic properties of the known oxo-bridged dimers allows us to predict the magnetic properties of unknown oxo-bridged dimers with trivalent 3d transition metal ions.

1. Introduction

The past two decades have witnessed the appearence of a large number of new and interesting polynuclear transition-metal complexes with paramagnetic constituents. These polynuclear complexes, apart from being of fundamental interest, serve as model systems in the study and development of molecular-based magnetic materials[1] as well as model compounds for metalloproteins in natural enzymatic systems.[2]

In the context of molecular-based magnetic materials the study of the properties of the low-nuclearity clusters has two main objectives: First, in these systems it is possible to get acquainted with the interactions between the nearest-neighbor metal centers.[3] These are the leading terms in determining the properties of more extended systems. And second, a detailed knowledge of the possible interactions is needed to predict which systems should be synthesized in order to get high magnetic ordering temperatures or other wanted properties.

Natural enzymatic systems containing paramagnetic ions have been characterized by their magnetic properties.[4] Some structural information is contained in a temperature-dependent magnetic susceptibility curve of a polynuclear metal complex, natural or not, and numerous magneto-structural correlations have been established.[5−7] The availability of suitable laboratory made model systems is essential in order to correlate the magnetic properties of natural enzymatic systems with important structural parameters.[7]

‡ Present address: Institute of Chemistry, Campusvej 55, University of Odense, DK-5230 Odense M, Denmark.

(1) Gatteschi, D. *Adv. Mat.* **1994**, *6*, 635.
(2) Armstrong, W. H.; Spool, A.; Papaefthymion, G. C.; Frenkel, R. B.; Lippard, S. J. *J. Am. Chem. Soc.* **1984**, *106*, 3653.
(3) Willet, R. D.; Gatteschi, D.; Kahn, O. *Magneto-Structural Correlations in Exchange Coupled Systems*; Proceedings of the NATO ASI; D. Reidel Publishing Co.; Dordrecht, Holland, 1985.
(4) Dawson, J. W.; Gray, H. B.; Hoenig, H. E.; Rossmann, G. R.; Schredder, J. M.; Wang, R-H. *Biochemistry* **1972**, *11*(3), 461.
(5) Crawford, V. H.; Richardson, H. W.; Wassen, J. R.; Hodgson, D. J.; Hatfield, W. E. *Inorg. Chem.* **1976**, *9*, 2107.
(6) Glerup, J.; Hodgson, D. J.; Pedersen, E. *Acta Chem. Scand.* **1983**, *A37*, 161.
(7) Weihe, H.; Güdel, H. U. *J. Am. Chem. Soc.* **1997**, *119*, 6539.
(8) Bodner, A.; Drüeke, S.; Wieghardt, K.; Nuber, B.; Weiss, J. *Angew. Chem.* **1990**, *102*, 60.
(9) Jeske, P.; Wieghardt, K.; Nuber, B. *Inorg. Chem.* **1994**, *29*, 47.
(10) Brand, S. G.; Edelstein, N.; Hawkins, C. J.; Shalimoff, G.; Snow, M. R. Tiekink, E. R. T. *Inorg. Chem.* **1990**, *29*, 434.
(11) Knopp, P.; Wieghardt, K.; Nuber, B.; Weiss, J.; Sheldrick, W. S. *Inorg. Chem.* **1990**, *29*, 363.
(12) Pedersen, E. *Acta Chem. Scand.* **1972**, *26*, 333.
(13) Güdel, H. U.; Dubicki, L. *Chem. Phys.* **1974**, *6*, 272.
(14) Glerup, J. *Acta Chem. Scand.* **1972**, *26*, 3775.
(15) Gafford, B. G.; O'Rear, C.; Zhang, J. H.; O'Connor, C. J.; Holwerda, R. A. *Inorg. Chem.* **1989**, *28*, 1720.
(16) Kipke, C. A.; Scott, M. J.; Gohdes, J. W.; Armstrong, W. H. *Inorg. Chem.* **1990**, *29*, 2193.
(17) Ziolo, R. F.; Stanford, R. H.; Rossmann, G. R.; Gray, H. B. *J. Am. Chem. Soc.* **1974**, *96*.
(18) Ou, C. C.; Wollmann, R. G.; Hendrickson, D. N.; Potenza, J. A.; Schugar, H. J. *J. Am. Chem. Soc.* **1978**, *100*, 4717.
(19) Hazell, A.; Jensen, K. B.; McKenzie, C. J.; Toftlund, H. *Inorg. Chem.* **1994**, *33*, 3127.
(20) Bodner, A.; Drüeke, S.; Wieghardt, K.; Nuber, B.; Weiss, J. *Angew. Chem.* **1990**, *102*, 60; *Angew. Chem., Int. Ed. Engl.* **1990**, *29*, 68.
(21) Wieghardt, K.; Köppen, M.; Nuber, B.; Weiss, J. *J. Chem. Soc., Chem. Commun.* **1986**, 1533.
(22) Knopp, P.; Wieghardt, K. *Inorg. Chem.* **1991**, *30*, 4061.
(23) Bond, M. R.; Czernuszewicz, R. S.; Dave, B. C.; Yan, Q.; Mohan, M.; Verastegue, R.; Carrano, C. J. *Inorg. Chem.* **1995**, *34*, 5857.
(24) Hotzelmann, R.; Wieghardt, K.; Flörke, U.; Haupt, H.-J.; Weatherburn, D. C.; Bonvoisin, J.; Blondin, G.; Girerd, J.-J. *J. Am. Chem. Soc.* **1992**, *114*, 1681.
(25) Martin, L. L.; Wieghardt, K.; Blondin, G.; Girerd, J-J.; Nuber, B.; Weiss, J. *J. Chem. Soc., Chem. Commun.* **1990**, 1767.
(26) Wieghardt, K.; Bossek, U.; Ventur, D.; Weiss, J. *J. Chem. Soc., Chem. Commun. 1985*, 347.
(27) Wieghardt, K.; Bossek, U.; Nuber, B.; Weiss, J.; Bonvoisin, J.; Corbella, M.; Vitols, S. E.; Girerd, J.-J. *J. Am. Chem. Soc.* **1988**, *110*, 7398.
(28) Bossek, U.; Wieghardt, K.; Nuber, B.; Weiss, J. *Inorg. Chim. Acta* **1989**, *165*, 123.
(29) Sheats, J. E.; Czernuszewicz, R. S.; Dismukes, G. C.; Rheingold, A. L.; Petrouleas, V.; Stubbe, J.; Armstrong, W. H.; Beer, R. H.; Lippard, S. J. *J. Am. Chem. Soc.* **1987**, *109*, 1435.
(30) Ménage, S.; Girerd, J.-J.; Gleizes, A. *J. Chem. Soc., Chem. Commun.* **1988**, 431.
(31) Vincent, J. B.; Folling, K.; Huffmann, J. C.; Christou, G. *Biochem. Soc. Trans.* **1988**, *16*, 822.
(32) Christou, G. *Acc. Chem. Res.* **1989**, *22*, 328.
(33) Chaudhuri, P.; Wieghardt, K.; Nuber, B.; Weiss, J. *Angew. Chem., Int. Ed. Engl.* **1985**, *24*, 778.

S0002-7863(97)03021-7 CCC: $15.00
Published on Web 03/17/1998

Table 1. Homonuclear Transition-Metal Dimers Containing the Linear, or Close to Linear, Unsupported Oxo Bridge[a]

$d^m d^n$	compd	r_{MO}/Å	ϕ/deg	J_{exp}/cm^{-1}	ref
d^1d^1	$[Me_3tacn(Cl)_2Ti]_2O$			≈0	8
	$[Me_3tacn(NCO)_2Ti]_2O$	1.838	180	15.6	9
	$[Me_3tacn(NCS)_2Ti]_2O$			11.2	9
d^2d^2	$\{[(bpy)_2(Cl)V]_2O\}^{2+}$	1.787	173.5	<−400	10
	$\{[Me_3tacn(acac)V]_2O\}^{2+}$	1.806	180	−224	11
d^3d^3	$\{[(NH_3)_5Cr]_2O\}^{4+}$	1.80	180	450	12−14
	$\{[tpa(NCS)Cr]_2O\}^{2+}$			509	15
	$\{[tpa(NC)Cr]_2O\}^{2+}$			580	15
d^4d^4	$[(NO_2saldien)Mn]_2O$	1.914, 1.757	168.4	240	16
$d^4(ls)d^4(ls)$	$\{[(NC)_5Mn]_2O\}^{6-}$	1.723	180	>870[b]	17
d^5d^5	$[(C_7H_2NClO_4)(H_2O)_2Fe]_2O$	1.773	180	214	18
	$\{[tpa(Cl)Fe]_2O\}^{2+}$	1.785	174.7	232	18

[a] The first and second column list the dimer electron configurations and complexes, respectively. *n* and *m* are the number of metal d electrons. ls = low-spin. The ligand abbreviations are as follows: Me_3tacn = *N*,*N*′,*N*″-trimethyl-1,4,7-triazacyclononane, bpy = bipyridine, NO_2 saldien = *N*,*N*′-bis(5-nitrosalicylidene)-1,7-(diamino)-3-azapentane, $C_7H_2NClO_4$ = 4-chloro-2,6-pyridinedicarboxylate, tpa = tris(2-pyridyl)amine. The third and fourth columns list the metal−oxygen(bridge) distances r_{MO} and the metal−oxygen(bridge)−metal angle ϕ, respectively. The fifth column gives the experimentally determined *J* values (eq 1). [b] The value of 870 cm^{-1} was calculated using the reported μ_{eff} value ($0.41\mu_B/Mn$ at room temperature) and assuming $g = 2$; due to unknown amounts of paramagnetic impurities this value is a lower limit for *J*.

The magnetic interactions between two metal ions in a polynuclear complex or in an extended magnetic lattice are mainly determined by the following parameters: (i) the electron configuration of the metal ions, (ii) the chemical nature of the bridging ligands, and (iii) the geometry of the bridging arrangement, i.e., metal−ligand distances and angles. The nature of the nonbridging ligands is considered less important and will be neglected in the present study.

In this paper, we present a theoretical study of the correlation of the magnetic properties of oxo-bridged transition metal dimers with the metal−(μ-oxo)−metal bridging angle. The study is based on the structural and magnetic properties of oxo-bridged trivalent transition-metal dimers reported in the literature. Linear and strongly bent homonuclear and heteronuclear dimers are included.

As representatives for the linear systems, we have included dimers bridged by a single oxide ion, and as representatives for the strongly bent systems we have included dimers containing the μ-oxobis(μ-carboxylato) bridging arrangement. We have chosen to include only those dimers in which the constituent monomeric metal centers are six coordinate. The magnetic and relevant structural properties for the linear and the strongly bent systems are presented in Tables 1 and 2, respectively.

The ground-state magnetic properties of all the dimers have been interpreted (see references cited in Tables 1 and 2) in terms of the so-called Heisenberg−Dirac−van Vleck (HDvV) effective Hamiltonian

$$\hat{H}_{HDvV} = J\hat{S}_A\hat{S}_B \qquad (1)$$

which sometimes appears in the form $-J\hat{S}_A\hat{S}_B$ or $-2J\hat{S}_A\hat{S}_B$. We choose the simpler form (eq 1) in which ferro- and antiferromagnetic interactions are represented by negative and positive *J* values, respectively.

The compounds listed in Tables 1 and 2 provide an ideal basis for an analysis and quantitative comparison. The linear systems in Table 1 represent six different dimer electron configurations including five configurations in which both metals have the high-spin configuration and one configuration in which both metals have the low-spin configuration. The linear systems exhibit a wide range from −400 cm^{-1} to at least 870 cm^{-1} of experimentally determined *J* values. The strongly bent systems in Table 2 represent nine different dimer electron configurations in which both metals have the high-spin electron configuration. Experimental *J* values range from −400 to 500 cm^{-1} in the bent systems. Notice that the compounds in Tables 1 and 2 represent two distinct groups of complexes. The metal−(μ-oxo)−metal angles are in the intervals 170−180° and 120−130° in Tables 1 and 2, respectively. Notice also that if there are several complexes representing an electron configuration in Table 1 or 2, the *J* values for these complexes fall in a relatively narrow range compared to the total spread in the *J* values.

By choosing only oxo-bridged dimers we do not vary the chemical nature of the bridging ligand. Thus, the electron configuration and the bridging geometry are the variable

Table 2. Homo- and Heteronuclear Trivalent Transition-Metal Dimers Containing the μ-Oxobis(μ-acetato) Bridging Arrangement[a]

$d^m d^n$	compd	r_{MO}/Å	ϕ/deg	J_{exp}/cm^{-1}	ref
d^1d^1	$[L'_2Ti_2(O)(\phi CO_2)_2]^{2+}$	1.82	122.7	500	20
d^2d^2	$[L'_2V_2(O)(acO)_2]^{2+}$	1.792	130.2	−400	21, 22
	$[L'_2V_2(O)(acO)_2]^0$			F[b]	23
d^2d^3	$[LL'VCr(O)(acO)_2]^{2+}$			−200	24
d^3d^3	$[L'_2Cr_2(O)(acO)_2]^{2+}$	1.850	121.0	56	25
d^3d^4	$[LL'CrMn(O)(acO)_2]^{2+}$			−10	24
d^3d^5	$[LL'CrFe(O)(acO)_2]^{2+}$			275	24
d^4d^4	$[L'_2Mn_2(O)(acO)_2]^{2+}$	1.810	119.9	−18	26, 27
	$[L_2Mn_2(O)(acO)_2]^{2+}$	1.788	119.9	F[c]	28
	$[L'_2Mn_2(O)(acO)_2]^0$	1.780	125.1	1	29
	$[LL'Mn_2(O)(acO)_2]^{2+}$			−14	24
	$[bpy_2(H_2O)_2Mn_2(O)(acO)_2]^{2+}$	1.783	122.9	6.8	30
	$[bpy_2Cl_2Mn_2(O)(acO)_2]^0$			8.2	31, 32
	$[bpy_2(N_3)_2Mn_2(O)(\phi CO_2)_2]^0$	1.802	122.0	−6.8	31, 32
d^4d^5	$[LL'MnFe(O)(acO)_2]^{2+}$			136	24
	$[L'LMnFe(O)(acO)_2]^{2+}$			126	24
d^5d^5	$[L'_2Fe_2(O)(acO)_2]^{2+}$	1.800	119.7	238	33, 34
	$[LL'Fe_2(O)(acO)_2]^{2+}$			207	24
	$[L'_2Fe_2(O)(acO)_2]^0$	1.784	123.6	242	35
	$[bpy_2Cl_2Fe_2(O)(acO)_2]^0$	1.785	123.9	264	36

[a] The first and second column list the dimer electron configuration and complexes, respectively. *m* and *n* are the number of d electrons. The ligand abbreviations are as follows: L = 1,4,7-triazacyclononane, L′ = *N*,*N*′,*N*″-trimethyl-1,4,7-triazacyclononane, L″ = hydridotrispyrazolylborate, bpy = 2,2′-bipyridine, acO = acetate, and ϕCO_2 = benzoate. The third and the fourth column give the metal−oxide(bridge) distance r_{MO} and the metal−oxide(bridge)−metal angle ϕ, respectively. The fifth column gives the experimentally determined *J* values (eq 1). [b] Strong ferromagnetic coupling. [c] Weak ferromagnetic coupling.

(34) Hartmann, J. A.; Rardin, R. L.; Chaudhuri, P.; Pohl, K.; Wieghardt, K.; Nuber, B.; Weiss, J.; Papaefthymion, G. C.; Frankel, R. B.; Lippard, S. J. *J. Am. Chem. Soc.* **1987**, *109*, 7387.

(35) Armstrong, W. H.; Lippard, S. J. *J. Am. Chem. Soc.* **1984**, *106*, 4632.

(36) Vincent, J. B.; Huffmann, J. C.; Christou, G.; Li, Q.; Nanny, M. A.; Hendrickson, D. N.; Fong, R. H.; Fish, R. H. *J. Am. Chem. Soc.* **1988**, *110*, 6898.

parameters to be explored. For the bridging geometry we assume the bridging angle to be most important, and we neglect the metal−oxygen distance. This is justified as follows: Several experimental and theoretical studies of the distance dependence of J have concluded that J is proportional to r^{-b} ($12 < b < 16$)[37,38] or proportional to $\exp(-br)$ ($7 < b < 8$).[7,39] r is the metal-bridging ligand distance. With the range of r values in Tables 1 and 2, this could account for a total variation in J of a factor 3. We are interested in the much more drastic effects, such as the change in J observed for the Ti dimers when the bridging geometry is changed from linear ($J \approx 0$ cm^{-1}) to strongly bent ($J \approx 500$ cm^{-1}), or the observed change in J in the linear systems when the electron configuration is changed from d^2-d^2 ($J \approx -400$ cm^{-1}) to d^3-d^3 (450 cm^{-1} $\leq J \leq$ 580 cm^{-1}). These order of magnitude changes are mainly due to different angles and electron configurations with the r dependence playing a minor role. The choice of this approximation will be fully justified by the results obtained in the present study. As a result of analyzing the magnetic properties of known dimers we will be able to predict the magnetic properties of new compounds.

Our paper is organized as follows: In section 2 we briefly summarize the results of ref 40 in which we reanalyzed the contributions from the various one-electron interactions to the J value. We introduce the model parameters, i.e., the transfer integrals and the charge-transfer energies. This section is brief since the model was elaborated in ref 40. In section 3, we specify which of the one-electron parameters are of importance for the magnetic properties of the compound types studied in this paper. In section 4, we express the J values in terms of the model parameters, and in section 5, we apply the model and analyze the magnetic properties of the linear and the bent systems separately. In section 6, we combine the two situations and analyze the magnetic properties of the linear and the bent systems in terms of a common set of angular overlap parameters.

2. The Model

Equation 1 can in many cases describe the energy level spectrum of the dimer ground state that determines the magnetic properties. As a result, many models have been developed that attempt to relate the effective parameter J value to more fundamental quantities.

Two distinct contributions to J were recognized in the early days:[41] (i) *kinetic exchange* (or *the second-order effect of virtual electron transfer between metal ions*), originating in a one-electron transfer process, and (ii) *potential exchange* due to first-order true two-center two-electron exchange interactions. It was estimated that kinetic exchange usually is the most dominating contribution to J in insulating transition metal systems. This has later been demonstrated to be a valid estimate in several semiempirical and ab initio studies of exchange-coupled dimers. True two-center two-electron exchange integrals have been estimated to make a ferromagnetic contribution of 10 cm^{-1} at most.[42−45] Considering the large positive and negative J values in Tables 1 and 2, we can safely neglect potential exchange and take into account only the kinetic exchange contributions to J.

In ref 40 we critically analyzed the quantitative contributions of kinetic exchange to J[46] using the model and assumptions from the older literature.[41] Some of the old formulas were substituted by corrected versions.

We consider a dimer AB containing the metals A and B. Let $S_A\Gamma_A$ and $S_B\Gamma_B$ be the single-ion ground terms of A and B arising from the ground electron configurations, here specified as $(a)^{N_A}$ and $(b)^{N_B}$, respectively. S_A is the spin quantum number and Γ_A is the relevant orbital representation. (a) represents a collection of orbitals centered on A, and N_A is the total number of electrons on A, and similarly for center B. The number of unpaired electrons on A and B are designated n_A and n_B, respectively. We thus have $S_A = n_A/2$ and $S_B = n_B/2$, since we are only interested in the ground terms of A and B. The a and b orbitals are not pure metal orbitals. They contain contributions from the bridging as well as the terminal ligands. These orbitals are chosen to be orthonormal in our model, i.e., any a orbital on A is orthogonal to any b orbital on B.

We are interested in the eigenvalue spectrum of the dimer functions $|S\Gamma M\gamma\rangle$ obtained from the direct product of the single-ion ground terms:

$$|S\Gamma M\gamma\rangle = ((a)^{N_A}S_A\Gamma_A) \otimes ((b)^{N_B}S_B\Gamma_B) \qquad (2)$$

S and Γ are spin and orbital dimer quantum numbers. M and γ are components of S and Γ, respectively. The S quantum numbers are good quantum numbers, since we neglect spin−orbit coupling. In the absence of an interaction between the centers A and B all the $(2S_A + 1)(2S_B + 1)$ functions of eq 2 are degenerate. Under the action of a one-electron interaction operator $\hat{V}_{AB}$ the functions in eq 2 can interact with the charge-transfer functions

$$|S'\Gamma'M'\gamma'\rangle = ((a)^{N'_A}S'_B\Gamma'_A) \otimes ((b)^{N'_B}S'_B\Gamma'_B) \qquad (3)$$

in which N'_A and N'_B differ from N_A and N_B, respectively, due to an electron transfer from A to B, or vice versa. The one-electron operator $\hat{V}_{AB}$ is specified by its one-electron matrix elements, i.e., the transfer integrals h_{ij} defined as

$$h_{ij} = \langle a_i|\hat{V}_{AB}|b_j\rangle \qquad (4)$$

The transfer integrals h_{ij} are our model parameters. In section 3 we will specify those transfer integrals that are of importance for the dimers in Tables 1 and 2.

The interaction matrix elements of $\hat{V}_{AB}$ between the ground and the charge-transfer terms are of the type

$$\langle S\Gamma M\gamma|\hat{V}_{AB}|S'\Gamma'M'\gamma'\rangle \qquad (5)$$

Due to the normal selection rules of one-electron operators we must have $N'_A = N_A \pm 1$ and $N'_B = N_B \mp 1$. This means that the charge-transfer electron configuration $(a)^{N'_A}(b)^{N'_B}$ is obtained from the ground electron configuration $(a)^{N_A}(b)^{N_B}$ by taking one electron from one center and restoring it on the other, or vice versa. We distinguish between four types of such one-electron transfers: (i) the electron is taken from a half-filled orbital and restored in a half-filled orbital, (ii) the electron is taken from a half-filled orbital and restored in an empty orbital, (iii) the electron is taken from a full orbital and restored in a half-filled

(37) Bloch, D. *J. Phys. Chem. Solids* **1966**, *27*, 881.
(38) Schrivastava, K. N.; Jaccarino, V. *Phys. Rev. B* **1976**, *13*, 299.
(39) Wang, C.; Fink, K.; Staemmler, V. *Chem. Phys.* **1995**, *201*, 87.
(40) Weihe, H.; Güdel, H. U. *Inorg. Chem.* **1997**, *36*, 3632.
(41) Anderson, P. W. *Phys. Rev.* **1959**, *115*, 2.
(42) Ballhausen, C. J.; Hansen, Å. E. *Trans. Faraday Soc.* **1965**, *61*, 631.
(43) Fink, K.; Fink, R.; Staemmler, V. *Inorg. Chem.* **1994**, *33*, 6219.
(44) Wang, C.; Fink, K.; Staemmler, V. *Chem. Phys.* **1995**, *192*, 25.
(45) Ceulemans, A.; Heylen, G. A.; Chibotaru, L. F.; Maes, T. L.; Pierloot, K.; Ribbing, C.; Vanquickenborne, L. C. *Inorg. Chim. Acta* **1996**, *251*, 15.
(46) Goodenough, J. B. *Magnetism and the Chemical Bond*; Interscience: New York, 1963.

orbital, and finally (iv) the electron is taken from a full orbital and restored in an empty orbital. In all four cases the value of the matrix element eq 5 can be expressed in terms of h_{ij}, n_A, n_B, and S.[40]

The zero-order energy difference between the charge-transfer functions (eq 3) and the ground-state functions (eq 2) is U.[41] The effect of $\hat{V}_{AB}$ by eq 5 on the ground-state functions will be studied to the accuracy of second order by nondegenerate perturbation theory. We find[40] that the four above-mentioned types of electron transfer contribute to the J value with

$$\text{(i)} \qquad \frac{2}{n_A n_B}\frac{h_{ij}^2}{U} \tag{6}$$

$$\text{(ii)} \qquad \frac{-2}{n_A(n_B+1)}\frac{h_{ij}^2}{U}\frac{I_{n_B+1}}{U} \tag{7}$$

$$\text{(iii)} \qquad \frac{-2}{(n_A+1)n_B}\frac{h_{ij}^2}{U}\frac{I_{n_A+1}}{U} \tag{8}$$

$$\text{(iv)} \qquad \frac{2}{(n_A+1)(n_B+1)}\frac{h_{ij}^2}{U}\frac{(I_{n_A+1}-I_{n_B+1})}{U} \tag{9}$$

Equations 6−9 are valid for an electron transfer from A to B. The expressions for the opposite electron transfer are obtained by interchanging the A and B indices. I_{n_k+1} (k = A or B) is a single-ion quantity that represents the one-center exchange interactions on center k in the charge-transfer electron configuration. More precisely, I_{n_k+1} is the first-order energy difference between the ground state and the first excited state deriving from the electron configuration with $n_k + 1$ unpaired electrons. To a good approximation I_{n_k+1} is proportional to $n_k + 1$

$$I_{n_k+1} = (n_k + 1)I \tag{10}$$

where I is a constant.[40] In ref 40 we presented an experimental and theoretical verification of this simple rule. For tri- and divalent 3d transition metals I is approximately 5000 cm^{-1}.[40] With only the experimental J values at our disposal, we are not able to determine the values of the individual parameters h_{ij}, U, and I_{n_k+1} in the model. We therefore define the effective model parameters h'_{ij} and I' as follows:

$$h'_{ij} \equiv \frac{h_{ij}^2}{U} \tag{11}$$

and

$$I'_{n_k+1} = (n_k + 1)I' \equiv \frac{I_{n_k+1}}{U} \tag{12}$$

In the theory outlined above, U is formally the energy of a metal to metal charge-transfer configuration. On this basis, we estimate that $I' = I/U$ can be as high as 1/10.[40]

3. One-Electron Parameters

In this section, we demonstrate how the one-electron two-center transfer integrals introduced above are correlated with ligand-field parameters in the angular overlap model (AOM). The linear and bent μ-oxo dimers are represented in Figure 1. For the linear systems we assume that the symmetry around each metal center is C_{4v} leading to D_{4h} or C_{4v} dimer symmetry

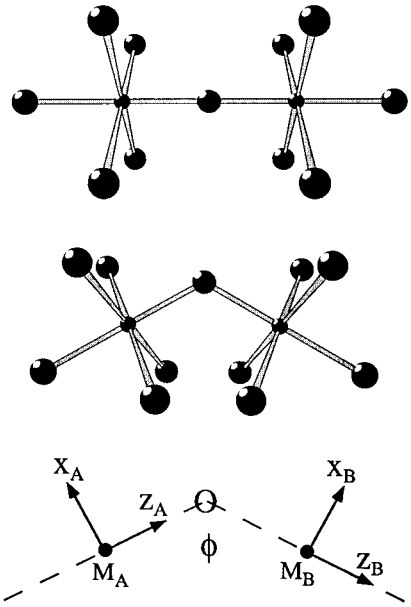

Figure 1. Schematic representation of the linear and bent oxo-bridged dimers and local coordinate systems used to define orbitals and interactions. The y_1 and y_2 axes point toward the viewer's eye. The plane containing the x_1, z_1, x_2, and z_2 axes is a mirror plane for both the linear and bent systems. Notice that the local z axes are defined in the C_{4v} symmetry and not in C_s.

for AB being homonuclear or heteronuclear, respectively. For the bent μ-oxobis(μ-carboxylato) systems we assume C_s local symmetries leading to C_{2v} or C_s dimer symmetries for AB being homonuclear or heteronuclear, respectively. The metal−(μ-oxo)−metal angle ϕ and the coordinate systems that will be used in the following are defined at the bottom of in Figure 1.

In these coordinate systems, we define the metal-rich orbitals: ξ_k, η_k, ζ_k, ϵ_k, and θ_k (k = A or B) with the same transformation properties as the products $(yz)_k$, $(zx)_k$, $(x^2 - y^2)_k$, $(xy)_k$, and $(2z^2 - x^2 - y^2)_k$, respectively. With these definitions the orbitals ξ_k, η_k, and ζ_k are the three components of the octahedral t_{2g} set, and the orbitals ϵ_k and θ_k are the components of the octahedral e_g set (see Figure 2).

3.1. Ligand Field Parameters. The energy ordering of the orbitals ξ_k, η_k, ζ_k, ϵ_k, and θ_k is of paramount importance for the ground-state magnetic properties.[47] With the knowledge of this energy ordering it is possible to determine the lowest energy electron configuration for a given system. In the following we use AOM arguments to determine the energy ordering of the single ion orbitals. The energy difference between the center of gravity of the ϵ_k, θ_k and the ξ_k, η_k, ζ_k set of orbitals is Δ; see Figure 2. For the type of ligands in Tables 1 and 2 it is known from the d−d spectra that Δ is in the range 15 000−20 000 cm^{-1}.[48] Due to the short metal−oxide (bridge) distance, the μ-oxo ion is mainly responsible for the low-symmetry ligand field components on each metal center. Oxide is a much stronger σ and π donor than the other ligands listed in Tables 1 and 2; see also section 6.[49,50] The parameters δ and γ, as defined in Figure 2, are thus both positive. Using known angular overlap parameters for oxide,[14,49,50] and assuming the

(47) Anderson, P. W. In *Magnetism*; Rado, G. T., Suhl, H., Eds.; Academic Press: New York, 1963, Vol. 1, Chapter 2.

(48) Glerup, J.; Mønsted, O.; Schäffer, C. E. *Inorg. Chem.* **1976**, *15*, 1399.

(49) Möller, A.; Hitchman, M. A.; Krausz, E.; Hoppe, R. *Inorg. Chem.* **1995**, *34*, 2684.

(50) Hitchman, M. A.; Stratemeier, H.; Hoppe, R. *Inorg. Chem.* **1988**, *27*, 2506.

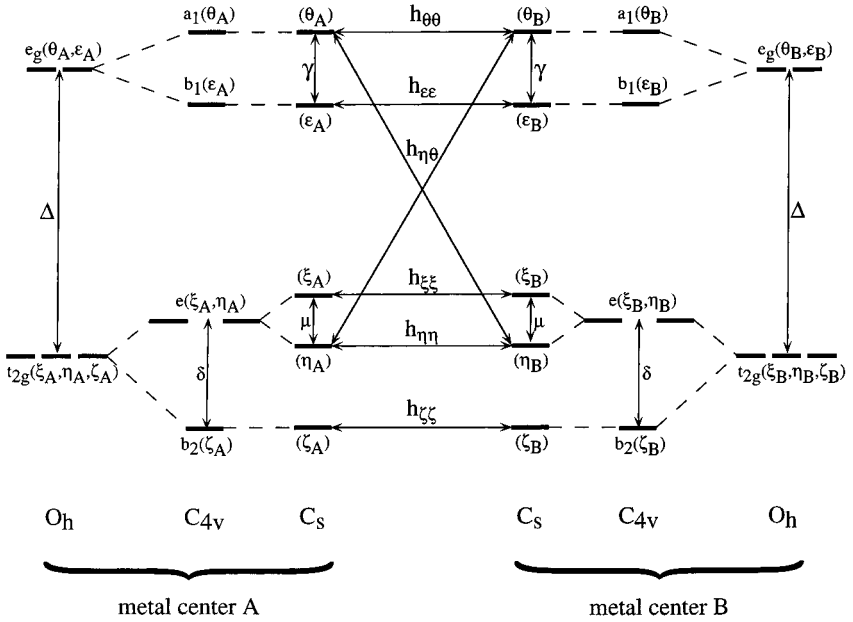

Figure 2. Schematic illustration of the one-electron parameters that are of importance for the magnetic properties of the systems studied in this paper. The left and the right part of the figure apply for metal centers A and B, respectively. The one-center (ligand field) parameters Δ, δ, μ, and γ are illustrated in the left and right part of the figure. The transfer integrals $h_{\zeta\zeta}$, $h_{\eta\eta}$, $h_{\xi\xi}$, $h_{\epsilon\epsilon}$, $h_{\theta\theta}$, and $h_{\eta\theta}$ are indicated by double arrows in the middle part. The O_h and C_{4v} one-electron energy levels are characterized by an irreducible representation of the respective point group, as well as the relevant one-electron function(s) spanning this irreducible representation.

other ligands to be pure σ donors with $e_\sigma \approx 7000$ cm^{-1}, we can estimate values of approximately 4000 and 3000 cm^{-1} for δ and γ, respectively. The magnitude of the parameter designated μ in Figure 2 is more difficult to estimate using angular overlap arguments. μ is, of course, zero for the linear dimers fulfilling the D_{4h} or C_{4v} symmetry criteria mentioned above. μ is not zero for the bent dimers. Most of the μ-oxo−bis(μ-carboxylato)-bridged dimers (Table 2) have three nitrogen donors in the nonbridging positions, i.e., two nitrogen atoms cis and one nitrogen trans to the bridging oxide, respectively. Hence, the holoedric symmetry around each metal center is close to D_{4h}, and we conclude that the parameter μ is much smaller than δ and γ.

3.2. Transfer Integrals. For the linear dimers we have five symmetry-allowed nonzero transfer integrals:

$$h_{\zeta\zeta} = \langle\zeta_A|\hat{V}_{AB}|\zeta_B\rangle = \langle\zeta_B|\hat{V}_{AB}|\zeta_A\rangle \quad (13)$$

$$h_{\eta\eta} = \langle\eta_A|\hat{V}_{AB}|\eta_B\rangle = \langle\eta_B|\hat{V}_{AB}|\eta_A\rangle \quad (14)$$

$$h_{\xi\xi} = \langle\xi_A|\hat{V}_{AB}|\xi_B\rangle = \langle\xi_B|\hat{V}_{AB}|\xi_A\rangle \quad (15)$$

$$h_{\epsilon\epsilon} = \langle\epsilon_A|\hat{V}_{AB}|\epsilon_B\rangle = \langle\epsilon_B|\hat{V}_{AB}|\epsilon_A\rangle \quad (16)$$

$$h_{\theta\theta} = \langle\theta_A|\hat{V}_{AB}|\theta_B\rangle = \langle\theta_B|\hat{V}_{AB}|\theta_A\rangle \quad (17)$$

For the bent systems the number of symmetry-allowed nonzero transfer integrals is larger and can be found as follows. On each metal center we have 3 and 2 orbitals transforming as a' and a'' in C_s, respectively. For a heteronuclear bent dimer we thus directly get the number of symmetry-allowed parameters as $(3 \times 3) + (2 \times 2) = 13$. This number reduces to 9 for the homonuclear bent dimer with C_{2v} symmetry.

In order to keep the number of parameters as low as possible, we do not retain all these transfer integrals in the model. By similar arguments as put forward in ref 24 we will include only the six transfer integrals (eqs 13−17) and an additional one:

$$h_{\eta\theta} = \langle\eta_A|\hat{V}_{AB}|\theta_B\rangle = \langle\theta_B|\hat{V}_{AB}|\eta_A\rangle \equiv \langle\theta_A|\hat{V}_{AB}|\eta_B\rangle = \langle\eta_B|\hat{V}_{AB}|\theta_A\rangle \quad (18)$$

The other ones can be neglected as shown below. All the transfer integrals included in our analysis are indicated by double arrows in Figure 2.

The relevant orbitals on the bridging oxide ion capable of σ and π interactions with the metal orbitals are the 2s and 2p orbitals. The metal orbitals θ_k, η_k, and ξ_k have σ, π, and π symmetry, respectively, with respect to the M−O axis and can thus interact. This justifies the inclusion of the transfer integrals $h_{\eta\eta}$, $h_{\xi\xi}$, $h_{\theta\theta}$, and $h_{\eta\theta}$. Oxygen has no low-lying orbitals with δ symmetry, and the two metal centers in the linear dimers are separated by 3.5−3.6 Å. The transfer integrals involving orbitals of δ symmetry with respect to the M−O−M axis in the linear systems, i.e., $h_{\zeta\zeta}$ and $h_{\epsilon\epsilon}$, are thus expected to be significantly smaller than the others for the linear geometry.

The transfer integrals depend on the metal−ligand(bridge) distances and on the bridging angle ϕ.[6,7,51] Here we are only interested in their ϕ dependence. The transfer integrals can be expressed in terms of AOM parameters. Using symmetry arguments we can qualitatively deduce how the transfer integrals depend on the M−O−M angle ϕ. The integrals involving the orbitals ξ_k, η_k, and θ_k are due to interactions via the bridging oxide. $h_{\xi\xi}$ is the out-of-plane π interaction in Figure 1 and thus expected to be independent of ϕ. $h_{\eta\eta}$ equals $h_{\xi\xi}$ for $\phi = 180°$ and equals zero for $\phi = 90°$. $h_{\eta\theta}$ equals zero for $\phi = 180°$. For $\phi \neq 180°$ the η orbital on one metal center and the θ orbital on the other metal center have finite overlaps with a common oxide p orbital. The parameter $h_{\eta\theta}$ is thus expected to have its maximum value for $\phi = 90°$. The orbitals θ_A and θ_B have common overlaps with the oxide s orbitals and the two p orbitals in the M−O−M plane. There are thus two contributions to $h_{\theta\theta}$: an s contribution that is independent on ϕ and a p

(51) Hay, P. J.; Thibeault, J. C.; Hoffmann, R. J. *J. Am. Chem. Soc.* **1975**, *97*, 4884.

contribution of different sign that drops to zero at $\phi = 90°$. By use of the AOM[52,53] we obtain the following quantitative ϕ dependencies of $h_{\xi\xi}$, $h_{\eta\eta}$, $h_{\eta\theta}$, and $h_{\theta\theta}$:

$$h_{\xi\xi}(\phi) = e_\pi \tag{19}$$

$$h_{\eta\eta}(\phi) = e_\pi(-\cos\phi) \tag{20}$$

$$h_{\eta\theta}(\phi) = \sqrt{e_\pi e_{\sigma p}}(\sin\phi) \tag{21}$$

$$h_{\theta\theta}(\phi) = e_{\sigma s} + e_{\sigma p}(\cos\phi) \tag{22}$$

The parameters e_π, $e_{\sigma p}$, and $e_{\sigma s}$ on the right hand side of eqs 19−22 are the ligand-field parameters of oxide in the AOM formulation. The angular dependencies of the two remaining transfer integrals $h_{\zeta\zeta}$ and $h_{\epsilon\epsilon}$ cannot be estimated with this simple method. In the strongly bent μ-oxobis(μ-carboxylato)-bridged systems the $h_{\epsilon\epsilon}$ and $h_{\zeta\zeta}$ interactions are through the σ and π framework, respectively, of the bridging carboxylates. In addition, direct overlap of the pure metal orbitals has also been considered to contribute to $h_{\zeta\zeta}$.[24] We thus expect $h_{\zeta\zeta}$ to be bigger than $h_{\epsilon\epsilon}$ in the bent systems.

4. Expressions for *J* Values

With the results from ref 40 briefly outlined in section 2 and the transfer integrals from section 3.2 we will now illustrate by an example how we obtain expressions for the ground state J value. Let A and B both have the ground electron configuration $\zeta\eta\xi$ leading to the dimer ground configuration $(\zeta_A\eta_A\xi_A)$-$(\zeta_B\eta_B\xi_B)$. We first consider charge-transfer states that arise from moving an electron from A to B. The three relevant charge transfer configurations $(\eta_A\xi_A)(\zeta_B^2\eta_B\xi_B)$, $(\zeta_A\xi_A)(\zeta_B\eta_B^2\xi_B)$, and $(\zeta_A\eta_A)(\zeta_B\eta_B\xi_B^2)$ are all obtained from the ground-state configuration by taking an electron from a half-filled orbital on A and restoring it in the corresponding half-filled orbital on B. The electronic terms arising from these three charge-transfer configurations can interact with the ground configuration terms. By use of eq 6, we find that the contribution to the J value from these three configurations is $2h_{\zeta\zeta}^2/(9U)$, $2h_{\eta\eta}^2/(9U)$, and $2h_{\xi\xi}^2/(9U)$, respectively. The terms arising from the charge-transfer configuration $(\zeta_A\xi_A)(\zeta_B\eta_B\xi_B\theta_B)$ contribute $-2h_{\eta\theta}^2/(12U)(I_4/U)$ to the J value according to eq 7. Contributions from other charge-transfer states are considered unimportant because the corresponding transfer integrals are small; see section 3.2. The electron transfers from B to A are exactly analogous and contribute the same energy terms. We thus obtain the following net expression for the net exchange parameter for d^3−d^3:

$$J = \frac{4}{9}\left(\frac{h_{\zeta\zeta}^2}{U} + \frac{h_{\eta\eta}^2}{U} + \frac{h_{\xi\xi}^2}{U}\right) - \frac{1}{3}\frac{h_{\eta\theta}^2}{U}\frac{I_4}{U} \tag{23}$$

By using this procedure for all the relevant electron configurations we obtain the expressions for the J values of the linear and bent systems collected in Tables 3 and 4, respectively. For the linear systems we only include the transfer integrals $h_{\xi\xi} = h_{\eta\eta}$ and $h_{\theta\theta}$, since $h_{\eta\theta}$ is zero by symmetry and the δ-type transfer integrals $h_{\epsilon\epsilon}$ and $h_{\zeta\zeta}$ are much smaller and thus neglected. For the bent systems we include all the transfer integrals (eqs 13−18).

The expression of J for the d^2−d^2 configuration in Tables 3 and 4 was obtained by a different procedure. The reason for this lies in the orbital degeneracy of the ^3E term deriving from the (ζ^1e^1) electron configuration in the local C_{4v} symmetry. We refer to refs 54 and 55 for a thorough discussion of this system.

Table 3. Theoretical J Values for Some Selected Electron Configurations in the Linear Geometry[a]

m, n	d^m	d^n	J_{calc}
1,1	ζ^1	ζ^1	0
1,2	ζ^1	ζ^1e^1	$-{}^1/_2h'_{\xi\xi}I'_2$
1,3	ζ^1	ζ^1e^2	$-{}^2/_3h'_{\xi\xi}I'_2$
1,4	ζ^1	$\zeta^1e^2\epsilon^1$	$-{}^1/_2h'_{\xi\xi}I'_2$
1,5	ζ^1	$\zeta^1e^2\epsilon^1\theta^1$	$-{}^2/_5h'_{\xi\xi}I'_2 - {}^1/_5h'_{\theta\theta}I'_2$
2,2[b]	ζ^1e^1	ζ^1e^1	$-h'_{\xi\xi}$
2,3	ζ^1e^1	ζ^1e^2	${}^2/_3h'_{\xi\xi}-{}^2/_9h'_{\xi\xi}I'_3$
2,4	ζ^1e^1	$\zeta^1e^2\epsilon^1$	${}^1/_2h'_{\xi\xi} - {}^1/_6h'_{\xi\xi}I'_3$
2,5	ζ^1e^1	$\zeta^1e^2\epsilon^1\theta^1$	${}^2/_5h'_{\xi\xi} - {}^2/_{15}h'_{\xi\xi}I'_3 - {}^2/_{15}h'_{\theta\theta}I'_3$
3,3	ζ^1e^2	ζ^1e^2	${}^8/_9h'_{\xi\xi}$
3,4	ζ^1e^2	$\zeta^1e^2\epsilon^1$	${}^2/_3h'_{\xi\xi}$
3,5	ζ^1e^2	$\zeta^1e^2\epsilon^1\theta^1$	${}^8/_{15}h'_{\xi\xi} - {}^1/_{10}h'_{\theta\theta}I'_4$
4,4	$\zeta^1e^2\epsilon^1$	$\zeta^1e^2\epsilon^1$	${}^1/_2h'_{\xi\xi}$
4,4	ζ^2e^2	ζ^2e^2	$2h'_{\xi\xi}$
4,5	$\zeta^1e^2\epsilon^1$	$\zeta^1e^2\epsilon^1\theta^1$	${}^2/_5h'_{\xi\xi} - {}^2/_{25}h'_{\theta\theta}I'_5$
5,5	$\zeta^1e^2\epsilon^1\theta^1$	$\zeta^1e^2\epsilon^1\theta^1$	${}^8/_{25}h'_{\xi\xi} + {}^4/_{25}h'_{\theta\theta}$

[a] The first column gives the number of d electrons on the two metal centers. The second and the third columns specify the electron configurations on the two metal centers. The orbital designations are the same as in Figure 2. The fourth column gives the theoretical J value according to section 3. We have included only the transfer integrals $h_{\xi\xi} \equiv h_{\eta\eta}$ and $h_{\theta\theta}$. [b] See refs 54 and 55 for details.

5. Comparison with Experiment

We will now apply the formalism developed above to the linear and bent systems separately. The linear and bent systems will be analyzed with the appropriate expressions from Tables 3 and 4, respectively. We assume that the linear systems can be described with one set of parameters, i.e., that the relevant parameters $h_{\xi\xi}$ and $h_{\theta\theta}$ do not depend on the electron configuration and are thus transferable between dimers containing different metals. Similarly for the bent systems. The quality of these assumptions will be tested. By analyzing the linear and bent systems separately we will be able to determine which parameters are important in the two types of geometry. In addition, we will see how much the corresponding parameters change on going from one geometry to the other.

The expressions for J_{calc} in Tables 3 and 4 are fitted to the J_{exp} values in Tables 1 and 2, respectively, with h'_{ij} and I' defined in eqs 11 and 12 as adjustable parameters. In order to do so, we minimize the residual function

$$R = \sum_{compounds} |J_{exp} - J_{calc}| \tag{24}$$

Notice that we minimize the sum of the absolute deviations. This is better suited for our purpose than χ^2 minimization, since χ^2 minimization is known to be rather sensitive to outliers in the data set.[56] We can immediately identify two outliers: The dichromium(III) dimer in Table 2 has a significantly longer r value than the other dimers. The divanadium(III) dimer in Table 2 has a significantly bigger M−O−M angle than the other bent dimers in Table 2. Some of the bridging geometries are represented by several complexes with the same electron configuration. In these cases we use their mean J value in the fit. No weighting scheme is used in the fit because experimental

(52) Schäffer, C. E. *Struct. Bonding* **1968**, *5*, 68.
(53) Atanasov, M.; Angelov, S. *Chem. Phys.* **1991**, *150*, 383.
(54) Weihe, H.; Güdel, H. U. *Chem. Phys. Lett.* **1996**, *261*, 123.
(55) Weihe, H.; Güdel, H. U.; Ward, T. R. Manuscript in preparation.
(56) Press, W. H.; Flannery, B. P.; Teukolsky, S. A.; Vetterling, W. T. *Numerical Recipes. The Art of Scientific Computing*; Cambridge University Press: Cambridge, U.K., 1986.

Table 4. Theoretical J Values for Some Selected Electron Configurations in the Bent Geometry[a]

m, n	d^m	d^n	J_{calc}
1,1	ζ	ζ	$4h'_{\zeta\zeta}$
1,2	ζ	$\zeta\eta$	$2h'_{\zeta\zeta} - {}^1/_2(h'_{\eta\eta} + h'_{\eta\theta})\,I'_2$
1,3	ζ	$\zeta\eta\xi$	${}^4/_3h'_{\zeta\zeta} - {}^1/_3(h'_{\eta\eta} + h'_{\xi\xi} + h'_{\eta\theta})\,I'_2$
1,4	ζ	$\zeta\eta\xi\epsilon$	$h'_{\zeta\zeta} - {}^1/_4(h'_{\eta\eta} + h'_{\xi\xi} + h'_{\epsilon\epsilon} + h'_{\eta\theta})\,I'_2$
1,5	ζ	$\zeta\eta\xi\epsilon\theta$	${}^4/_5h'_{\zeta\zeta} - {}^1/_5(h'_{\eta\eta} + h'_{\xi\xi} + h'_{\epsilon\epsilon} + h'_{\theta\theta} + h'_{\eta\theta})\,I'_2$
2,2[b]	$\zeta\eta$	$\zeta\xi$	$h'_{\zeta\xi} - (h_{\xi\xi}h_{\eta\eta})' - {}^1/_3h'_{\eta\theta}\,I'_3$
2,2[b]	$\zeta\eta$	$\zeta\eta$	$h'_{\zeta\zeta} + h'_{\eta\eta} - {}^2/_3h'_{\eta\theta}\,I'_3$
2,2[b]	$\zeta\xi$	$\zeta\xi$	$h'_{\zeta\zeta} + h'_{\xi\xi}$
2,3	$\zeta\eta$	$\zeta\eta\xi$	${}^2/_3(h'_{\zeta\zeta} + h'_{\eta\eta}) - {}^2/_9(h'_{\xi\xi} + h'_{\eta\theta})\,I'_3 - {}^1/_4h'_{\eta\theta}\,I'_4$
2,4	$\zeta\eta$	$\zeta\eta\xi\epsilon$	${}^1/_2(h'_{\zeta\zeta} + h'_{\eta\eta}) - {}^1/_6(h'_{\xi\xi} + h'_{\epsilon\epsilon} + h_{\eta\theta})\,I'_3 - {}^1/_5h'_{\eta\theta}\,I'_5$
2,5	$\zeta\eta$	$\zeta\eta\xi\epsilon\theta$	${}^2/_5(h'_{\zeta\zeta} + h'_{\eta\eta} + h'_{\eta\theta}) - {}^2/_{15}(h'_{\xi\xi} + h'_{\epsilon\epsilon} + h'_{\theta\theta} + h'_{\eta\theta})\,I'_3$
3,3	$\zeta\eta\xi$	$\zeta\eta\xi$	${}^4/_9(h'_{\zeta\zeta} + h'_{\eta\eta} + h'_{\xi\xi}) - {}^1/_3h'_{\eta\theta}\,I'_4$
3,4	$\zeta\eta\xi$	$\zeta\eta\xi\epsilon$	${}^1/_3(h'_{\zeta\zeta} + h'_{\eta\eta} + h'_{\xi\xi}) - {}^1/_8(h'_{\epsilon\epsilon} + h'_{\eta\theta})\,I'_4 - {}^2/_{15}h'_{\eta\theta}\,I'_5$
3,5	$\zeta\eta\xi$	$\zeta\eta\xi\epsilon\theta$	${}^4/_{15}(h'_{\zeta\zeta} + h'_{\eta\eta} + h'_{\xi\xi} + h'_{\eta\theta}) - {}^1/_{10}(h'_{\epsilon\epsilon} + h'_{\theta\theta} + h'_{\eta\theta})\,I'_4$
4,4	$\zeta\eta\xi\epsilon$	$\zeta\eta\xi\epsilon$	${}^1/_4(h'_{\zeta\zeta} + h'_{\eta\eta} + h'_{\xi\xi} + h'_{\epsilon\epsilon}) - {}^1/_5h'_{\eta\theta}\,I'_5$
4,4	$\zeta^2\eta\xi$	$\zeta^2\eta\xi$	$h'_{\eta\eta} + h'_{\xi\xi} - {}^2/_3h'_{\eta\theta}\,I'_3$
4,5	$\zeta\eta\xi\epsilon$	$\zeta\eta\xi$	${}^1/_5(h'_{\zeta\zeta} + h'_{\eta\eta} + h'_{\xi\xi} + h'_{\epsilon\epsilon} + h'_{\eta\theta}) - {}^2/_{25}(h'_{\theta\theta} + h'_{\eta\theta})\,I'_5$
5,5	$\zeta\eta\xi\epsilon\theta$	$\zeta\eta\xi\epsilon\theta$	${}^4/_{25}(h'_{\zeta\zeta} + h'_{\eta\eta} + h'_{\xi\xi} + h'_{\epsilon\epsilon} + h'_{\theta\theta} + 2h'_{\eta\theta})$

[a] The first column gives the number of d electrons on the two metal centers. The second and the third column specify the electron configurations on the two metal centers. The orbital designations are the same as in Figure 2. The fourth column gives the theoretical J value according to section 3. We have included the transfer integrals eqs 13−18. We defined $(h_{ij}h_{kl})' \equiv h_{ij}h_{kl}/U$. [b] See refs 54 and 55 for details.

Table 5. Comparison of the Experimental and Calculated J Values for the Linear Systems[a]

	J_{exp}/cm^{-1}	J_{calc}/cm^{-1}
d^1d^1	9	0
d^2d^2	−400	−480
d^3d^3	513	427
d^4d^4(hs)	240	240
d^4d^4(ls)	870	960
d^5d^5	210	210

[a] The J_{calc} values were calculated with the expressions from Table 3 and the parameter values from Table 7, column c, as described in section 5.1.

Table 6. Comparison of the Experimental and Calculated J Values for the Bent Systems[a]

	J_{exp}/cm^{-1}	J_{calc}/cm^{-1}
d^1d^1	500	496
d^2d^2	−400	−228
d^2d^3	−200	−202
d^3d^3	56	63
d^3d^4	−10	20
d^3d^5	275	277
d^4d^4	−4	−5
d^4d^5	131	190
d^5d^5	237	311

[a] The J_{calc} values were calculated with the expressions from Table 4 and the parameter values from Table 7, column d, as described in section 5.2.

Table 7. Model Parameters Obtained by Minimizing eq 24[a]

parameters[b]	linear[c]	bent[d]	linear + bent[e]
$h_{\xi\xi}'$	480	407	−
$h_{\eta\eta}'$	480	85	−
$h_{\zeta\zeta}'$	−	124	−
$h_{\theta\theta}'$	352	10	−
$h_{\eta\theta}'$	−	655	−
I'	−	0.25	0.29
e_π'	−	−	20.86
$e_{\sigma s}'$	−	−	18.42
$e_{\sigma p}'$	−	−	39.46
x'	−	−	0.19

[a] A − means that this parameter was not included in the fit. See sections 5 and 6 for details. [b] The parameters $h'_{\xi\xi}$, $h'_{\eta\eta}$, $h'_{\zeta\zeta}$, $h'_{\theta\theta}$ and $h'_{\eta\theta}$ are in units of cm^{-1}. I' is dimensionless, and e'_π, $e'_{\sigma s}$, $e'_{\sigma p}$ and x' are in units of $(cm^{-1})^{1/2}$. [c] See section 5.1. [d] See section 5.2. [e] See section 6.

J values are rarely reported with an error bar. Using this procedure, two and six independent parameters were adjusted in the fits of the linear and bent systems, respectively.

5.1. Linear Systems. A comparison of the experimental and calculated J values is given in Table 5. The values of the parameters $h'_{\xi\xi} = h'_{\eta\eta}$ and $h'_{\theta\theta}$ which minimized eq 24 are collected in Table 7, column c. Inclusion of the δ symmetry transfer integrals $h_{\zeta\zeta}$ and $h_{\epsilon\epsilon}$ only marginally improved the fit. $h'_{\zeta\zeta}$ and $h'_{\epsilon\epsilon}$ values were 5−10 times smaller than those of $h'_{\xi\xi}$ and $h'_{\theta\theta}$. This justifies the neglect of these parameters in the linear geometry, as expected theoretically (see also section 3.2). The parameter I' cannot be obtained from the linear systems since none of the relevant expressions in Table 3 depend on this parameter. The reason for this is the high D_{4h} symmetry and the presence of only homonuclear dimers in Table 1.

The agreement of experimental and calculated J values in Table 5 is excellent. The enormous experimental variation from strongly ferromagnetic coupling in d^2-d^2 to uncoupled d^1-d^1 to strongly antiferromagnetic coupling in d^4(ls)-d^4(ls) is very well reproduced. The first five J_{calc} values in Table 5 were calculated with only one parameter, namely $h'_{\eta\eta} = h'_{\xi\xi}$. The relative magnitudes of the experimental J values for the five first electron configurations follow closely the theoretically expected relative magnitudes, namely $0 : -1 : {}^8/_9 : {}^1/_2 : 2$. We therefore conclude that the model parameter $h_{\xi\xi} = h_{\eta\eta}$ is transferable between linear dimers with different electron configurations.

5.2. Bent Systems. A comparison of the experimental and calculated J values is given in Table 6. The parameter values that minimized eq 24 are collected in Table 7, column d. We initially included all the transfer integrals listed in Table 4. Since the δ-symmetry parameter $h'_{\epsilon\epsilon}$ came out with a very low value of 3 cm^{-1} and thus only marginally influenced the overall result we chose to neglect it. Also in this series the agreement between experimental and calculated J values is very good. In particular, the experimentally observed variation between ferro- and antiferromagnetic coupling along the series is well reproduced. At this point one might argue that the good agreement is the result of the relatively large number of parameters (six) compared to the number of experimental J values (nine). This is not so. In sections 5.3 and 6 we will show that the parameters of the linear and bent systems are physically connected and can be reduced to one set of five parameters.

5.3. Discussion of the Angular Variation of the Parameters. In the following comparison of the parameter values obtained from the linear and the bent geometries we assume $\phi = 180°$ for the linear oxo-bridged species and $\phi = 120°$ for the bent oxobis(carboxylato)-bridged species. We first discuss the three transfer integrals that the linear and bent systems have in common, namely $h_{\xi\xi}$, $h_{\eta\eta}$, and $h_{\theta\theta}$.

The effective parameter $h'_{\xi\xi}$ decreases from 480 to 407 cm^{-1} on bending from $\phi = 180°$ to $\phi = 120°$. For the transfer integral $h_{\xi\xi}$ we get

$$\frac{h_{\xi\xi}(180°)}{h_{\xi\xi}(120°)} = \sqrt{\frac{h'_{\xi\xi}(180°)}{h'_{\xi\xi}(120°)}} = 1.08 \qquad (25)$$

The agreement with the theoretical expectation based on the AOM that $h_{\xi\xi}$ is independent of ϕ (see eq 19 is thus excellent.

The value of $h_{\eta\eta}$ is strongly affected by the change in bridging geometry. The effective parameter $h'_{\eta\eta}$ decreases from 480 cm^{-1} (linear) to 82 cm^{-1} (bent). For the transfer integral $h_{\eta\eta}$ we get

$$\frac{h_{\eta\eta}(180°)}{h_{\eta\eta}(120°)} = \sqrt{\frac{h'_{\eta\eta}(180°)}{h'_{\eta\eta}(120°)}} = 2.38 \qquad (26)$$

Theoretically, this ratio equals $cos(180)/cos(120) = 2$; see eq 20. Equation 26 thus indicates a slightly stronger decrease than expected, but again the trend is very well reproduced by eq 20. We note here that our findings (eqs 25 and 26) agree well with an extended Hückel estimate of the angular dependencies of these parameters (see Figure 12 in ref 24).

$h'_{\theta\theta}$ has quite a pronounced angular dependence, since it decreases from 352 to 10 cm^{-1}, i.e., almost zero, on bending from $\phi = 180°$ to $\phi = 120°$. We notice here that $h'_{\theta\theta}(180°)$ is determined solely based on the linear ferric dimers from Table 1. Therefore, too much significance should not be put onto the absolute value of $h'_{\theta\theta}(180°)$ in the present discussion of its angular variation. The big value for $h'_{\theta\theta}(180°) = 352$ cm^{-1}, which is comparable in magnitude with $h'_{\xi\xi}$, is in contrast to the results obtained using extended Hückel calculations.[24] There $h_{\theta\theta}$ was found negligible at all angles. Our identification of the $\theta\theta$ interaction as an important one for $\phi = 180°$ and less important for $\phi = 120°$ agrees with an SCF-Xα-SW calculation[57] on a linear and bent oxo-bridged ferric dimer.

The most dramatic ϕ dependence is found in the parameter $h_{\eta\theta}$. The effective parameter $h'_{\eta\theta}$ increases from zero in the linear geometry to 655 cm^{-1} for $\phi = 120°$. From this value of $h'_{\eta\theta} = 655$ cm^{-1} and eq 21 we find that $e_\pi e_{\sigma p}/U = 873$ cm^{-1}. This compares very well with $(e_\pi/\sqrt{U})(e_{\sigma p}/\sqrt{U}) = 859$ cm^{-1} where $e_\pi/\sqrt{U}$ is obtained from $h'_{\xi\xi}(180°)$ and $e_{\sigma p}/\sqrt{U}$ is obtained from $h'_{\theta\theta}(180°)$ and $h'_{\xi\xi}(120°)$. This clearly shows the validity of eq 21.

The value of the parameter $h_{\zeta\zeta}$ cannot simply be connected with the values of $h_{\xi\xi}$, $h_{\eta\eta}$, $h_{\eta\theta}$, and $h_{\theta\theta}$, and it cannot be interpreted in terms of AOM parameters for the bridging oxide. The reason for this is that the ζ orbitals do not interact via the intervening oxide ion. There are contributions from the direct overlap of the relevant metal orbitals and superexchange contributions involving the bridging carboxylates.[24] The effective parameter $h'_{\zeta\zeta}$ increases from zero to 124 cm^{-1} on lowering ϕ from 180° to 120°. This parameter contributes antiferromagnetically to the J value of all the bent compounds; see the expressions for the J values in Table 4. This effect is most pronounced for the dititanium(III) complex due to the factor $2/n_A n_B$ in eq 6.

There is a remarkable agreement between our parameter values, which are extracted from the experimental J values by use of a minimum of formalism, and the corresponding parameter values recently obtained by sophisticated SCF-Xα-SW calculations on linear and bent oxo-bridged ferric dimers.[57] For the linear geometry we find that the transfer integrals $h_{\xi\xi}$:$h_{\theta\theta}$:$h_{\epsilon\epsilon}$:$h_{\zeta\zeta}$ have the relative magnitudes 22:19:0:0. Reference 57 finds the values 3916:2911:97:40[58] for these transfer integrals, respectively. For the bent geometry our ratios of the transfer integrals $h_{\xi\xi}$:$h_{\zeta\zeta}$:$h_{\eta\eta}$:$h_{\theta\theta}$:$h_{\epsilon\epsilon}$ are 20:11:9:3:0 compared to the values 4569:1436:1057:870:423 found by refs 57 and 58. This agreements clearly tells us that our treatment is sound.

In section 2 it was theoretically estimated that the value of the parameter I' should be at most 1/10. The value of 0.25 obtained in our fits is higher, and this will be discussed in section 6.

6. Angle Dependence of the Transfer Integrals and the *J* Values

In this section we connect the linear and bent systems by relating the parameters determined in section 5 to the same set of AOM parameters. The model is based on the results obtained in the previous section. In addition to accounting for the magnetic properties of the compounds listed in Tables 1 and 2 it will be used to predict the magnetic properties of new dimers not yet included in the tables.

Expressions for the J_{calc} values are taken from Table 4, and the four transfer integrals $h_{\xi\xi}$, $h_{\eta\eta}$, $h_{\eta\theta}$, and $h_{\theta\theta}$ are expressed in terms of the three AOM parameters e_π, $e_{\sigma p}$, and $e_{\sigma s}$ by eqs 19−22, respectively. For the transfer integral $h_{\zeta\zeta}$, which cannot be expressed in terms of AOM parameters, we assume a linear variation with ϕ in the angular interval $120° \le \phi \le 180°$ as follows:

$$h_{\zeta\zeta} = x(\phi - 180°) \qquad (27)$$

With these definitions of the transfer integrals the expressions for J_{calc} from Table 4 become identical with the corresponding expressions from Table 3 for $\phi = 180°$.

As an illustration of the procedure we show with an example how the expressions for J_{calc} from Table 4 can be expressed in terms of the parameters e_π, $e_{\sigma p}$, $e_{\sigma s}$, x, I, and U. For a vanadium−chromium dimer d^2−d^3 we find the following theoretical expression for J from Table 4:

$$J_{calc} = \frac{2}{3}\left(\frac{h^2_{\zeta\zeta}}{U} + \frac{h^2_{\eta\eta}}{U}\right) - \frac{2}{9}\left(\frac{h^2_{\xi\xi}}{U} + \frac{h^2_{\eta\theta}}{U}\right)\frac{I_3}{U} - \frac{1}{4}\frac{h^2_{\eta\theta}}{U}\frac{I_4}{U} \qquad (28)$$

Making use of eqs 12, 19−22, and 27 we find

$$J_{calc} = \frac{2}{3}\frac{x^2(180-\phi)^2}{U} + \frac{2}{3}\frac{e^2_\pi}{U}\left((\cos\phi)^2 - \frac{I}{U}\right) - \frac{5}{3}\frac{e_\pi e_{\sigma p}}{U}(\sin\phi)^2\frac{I}{U} \qquad (29)$$

The ϕ dependence of the J values for the other electron

(57) Brown, C. A.; Remar, G. J.; Musselmann, R. L.; Solomon, E. I. *Inorg. Chem.* **1995**, *34*, 688.

(58) The numbers quoted from ref 57 are obtained from Table 2A,B (in ref 57) for the linear and bent dimers, resectively. The transfer integrals quoted by us are calculated from these tables as half the energy difference between the symmetric and the antisymmetric linear combination of corresponding orbitals, i.e., $h_{aa} = {}^1/_2\ [E[(1/\sqrt{2})(a_1 + a_2)] - E[(1/\sqrt{2})(a_1 - a_2)]]$.

configurations is found similarly. From eq 29 we see that the parameters which can be determined are

$$e'_\pi = \frac{e_\pi}{\sqrt{U}} \tag{30}$$

$$e'_{\sigma p} = \frac{e_{\sigma p}}{\sqrt{U}} \tag{31}$$

$$e'_{\sigma s} = \frac{e_{\sigma s}}{\sqrt{U}} \tag{32}$$

$$x' = \frac{x}{\sqrt{U}} \tag{33}$$

and

$$I' = \frac{I}{U} \tag{34}$$

The parameters $e_{\sigma s}$ and $e_{\sigma p}$ occur separately in the expressions for J_{calc} and can thus be determined separately. This is in contrast to d−d excitation energies in optical spectroscopy, where a separation of the σ interaction into s and p contributions is not possible.

The five model parameters e'_π, $e'_{\sigma p}$, $e'_{\sigma s}$, x' and I' are now extracted from the experimental J values in Tables 5 and 6 by again minimizing the function (eq 24). As input values we used corresponding mean values of J_{exp} and ϕ. The J_{exp} values that were used are given in Tables 5 and 6. The parameter values thus obtained are collected in the last column of Table 7. Before we compare the experimental and calculated J values we discuss the obtained parameter values.

From Table 7 we find the following ratio of AOM parameters for oxide coordinated to trivalent 3d transition metals

$$e_{\sigma p}:e_\pi:e_{\sigma s} \approx 2.1:1.1:1.0 \tag{35}$$

A very similar ratio, namely 2.5:1.0:1.0, was found in a previous analysis of 32 oxo-bridged iron(III) dimers.[7] It is remarkable that our present study, which considers a large number of different metal ions and electron configurations but neglects the r dependence of J, arrives at about the same result as a comprehensive study of Fe^{3+} dimers.[40] This clearly shows the dominant effect of the bridging angle and the transferability of the one-electron parameters.

At this point it is useful to recall some known ligand-field AOM parameters for oxide[14]

$$e_\pi \approx 4000\ cm^{-1} \tag{36}$$

This rather high value is supported by analysis of single-crystal absorption spectra of oxo-coordinated Ni^+ and Ni^{2+} species, in which e_π values of 3000 and 3500 cm^{-1}, respectively, were determined.[49,50] On the basis of eq 35 we can thus estimate the $e_{\sigma p}$ and $e_{\sigma s}$ AOM parameters for oxide coordinated to trivalent 3d transition metal ions:

$$7500\ cm^{-1} < e_{\sigma p} < 8500\ cm^{-1} \tag{37}$$

and

$$3000\ cm^{-1} < e_{\sigma s} < 4000\ cm^{-1} \tag{38}$$

Since $e_\sigma = e_{\sigma p} + e_{\sigma s}$ we consequently have

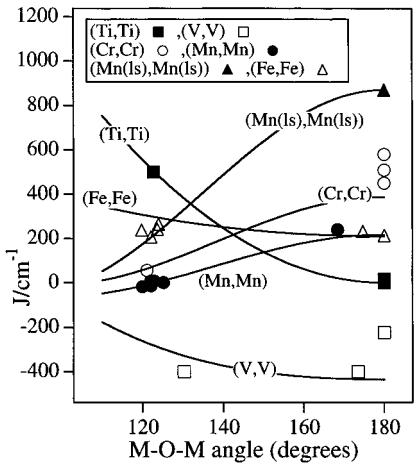

Figure 3. Comparison of the ϕ dependence of J_{calc} with J_{exp} for the homonuclear complexes in Tables 1 and 2. All the calculated J values (solid lines) were calculated with the parameters from Table 7 (last column) as described in section 6.

$$10\ 500\ cm^{-1} < e_\sigma < 12\ 500\ cm^{-1} \tag{39}$$

In ruby (Cr^{3+}-doped Al_2O_3) $\Delta = 3e_\sigma - 4e_\pi$ is approximately 18 000 cm^{-1}. This is in excellent agreement with the above estimates.

The parameter $h_{\zeta\zeta}$ is proportional to x according to eq 27 and cannot be discussed within the framework of the AOM. This parameter is essential for the antiferromagnetic coupling of the bent Ti dimer. It also adds an antiferromagnetic contribution to all the other bent dimers. The contribution of the $\zeta\zeta$ interaction pathway to the J value decreases drastically from the bent TiTi dimers ($4h'^2_{\zeta\zeta} = 500\ cm^{-1}$) to the bent FeFe dimers ($4h'^2_{\zeta\zeta}/25 = 20\ cm^{-1}$). We neglected this parameter in a previous analysis of the magnetic properties of oxo-bridged ferric dimers.[7]

In section 2 we estimated theoretically that the value of the parameter I' should not be higher than 1/10. Our values in Table 7 of 0.25 and 0.29 clearly exceed this limit. This discrepancy may have several causes. The most important in our view is the following. In the original theory of Anderson[41] U in eqs 6−9 is the energy required to transfer an electron from metal A to metal B. That is the basis of the estimate $I' \leq 1/10$. However, besides the metal-to-metal charge transfer also the oxygen-to-metal charge transfer can contribute to J.[59] As a consequence, the factor $(1/U)$ in eq 6 should be replaced by $(1/U + 1/E_{ct})$ where E_{ct} is the oxide-to-metal charge transfer energy.[59] More complicated, but similar, expressions should be substituted for $(1/U^2)$ in eqs7−9.[60] Since oxygen-to-metal charge-transfer transitions occur at lower energies than metal-to-metal charge-transfer transitions, the effective U values will thus be significantly smaller than the A → B electron-transfer energy. This leads to higher effective ratio $I' = I/U$ (eq 12).

A graphical comparison of the experimental and calculated ϕ dependence of J for the homonuclear dimers from Tables 1 and 2 is presented in Figure 3. The agreement using the same parameter set for all the examples is excellent. Both the variation from ferro- to antiferromagnetic interactions and the strongly varying ϕ dependences are well reproduced for all the electron configurations. The r dependence, which we have neglected in our model, is obviously a minor factor in this overall analysis.

(59) Zaanen, J.; Sawatzky, G. A. *Can. J. Phys.* **1987**, *65*, 1262. Geertsma, W. Physica B **1990**, *164*, 241.

(60) Weihe, H.; Güdel, H. U. Unpublished results.

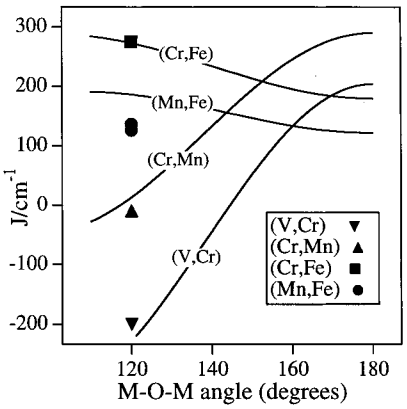

Figure 4. Comparison of the ϕ dependence of J_{calc} with J_{exp} for the heteronuclear complexes in Table 2. All the calculated J values (solid lines) were calculated with the parameters from Table 7 (last column) as described in section 6.

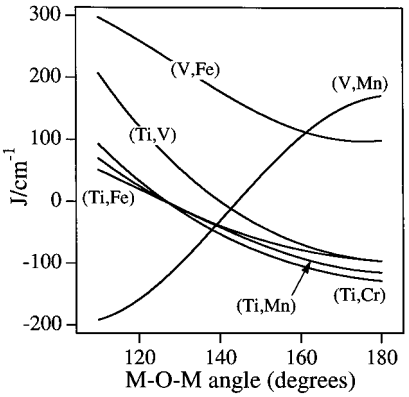

Figure 5. Calculated J values for some unknown μ-oxo-bridged dimetal(III) dimers. All the calculated J values (solid lines) were calculated with the parameters from Table 7 (last column) as described in section 6.

A graphical comparison of the calculated ϕ dependence of J with the experimental values for the bent heteronuclear dimers from Table 2 is given in Figure 4. So far, only heteronuclear dimers in the strongly bent geometry have been reported, e.g., as oxobis(carboxylato)-bridged dimers. But Figure 4 clearly tells us what we can expect when the heteronuclear dimers are straightened out. The J values of the CrFe and MnFe dimers will show only a weak ϕ dependence, and they will be antiferromagnetic for all ϕ values. The angle variation of the J values of the VCr and CrMn dimers will be more pronounced. The exchange interaction in these systems is predicted to change from strongly and weakly ferromagnetic, respectively, to both strongly antiferromagnetic in going from the bent to the linear geometry.

From the excellent agreement between experimental and calculated J values and their ϕ dependence in Figures 3 and 4 we conclude that the assumption of transferability of the model parameters between electron configurations is a good one. However, this is only valid as long as the metals between which parameters are transferred are isovalent. Three of the model parameters are essentially AOM ligand-field parameters, and it is well known that these are rather oxidation state dependent.

It is now tempting to take the next obvious step. In Figure 5 we have calculated the J values for six unknown oxo-bridged heteronuclear dimers of trivalent 3d transition-metal ions. From Figure 5 we can predict that linear oxo-bridged TiV, TiCr, TiMn, and TiFe dimers will show moderately strong ferromagnetic interactions that become all antiferromagnetic upon bending. Oxo-bridged VMn dimers will show the opposite variation, namely ferromagnetic interaction in the bent geometry and antiferromagnetic interaction in the linear geometry. And finally, oxo-bridged VFe dimers are predicted to be antiferromagnetic at all angles.

In conclusion, we have shown that it is possible to account for the magnetic properties of linear and bent homo- and heteronuclear trivalent transition-metal dimers with one oxo bridge by use of very simple concepts and formalisms. The recently developed formalism[40] that was briefly summarized in section 2 was shown to be a sound basis for the correct comparison of ground-state magnetic properties. An important step in our procedure is the connection of the transfer integrals occurring in the formulas for J with the angular overlap model parameters occuring in the ligand-field theory. In addition to accounting for the magnetic properties of a large number of oxo-bridged transition-metal dimers, our model allows a prediction of the properties of unknown complexes and their dependence on the bridging angle.

Acknowledgment. This work was financially supported by a Human Capital and Mobility fellowship from the EU (CHBICT941169) and the Swiss National Science Foundation.

JA973021A